

Solving Large Rank-Deficient Linear Least-Squares Problems on Shared-Memory CPU Architectures and GPU Architectures

Mónica Chillarón¹, Gregorio Quintana-Ortí², Vicente Vidal³, and Per-Gunnar Martinsson⁴

¹ *Dpto. de Sistemas Informáticos y Computación, Universitat Politècnica de València, 46022-València, Spain. email: mmichipr@inf.upv.es*

² *Dpto. de Ingeniería y Ciencia de Computadores, Universitat Jaume I de Castellón, 12071-Castellón, Spain. email: gquintan@uji.es*

³ *Dpto. de Sistemas Informáticos y Computación, Universitat Politècnica de València, 46022-València, Spain. email: vvidal@dsic.upv.es*

⁴ *Dept. of Mathematics, 2515 Speedway, University of Texas at Austin, 78712, Austin, Texas, USA. email: pgm@oden.utexas.edu*

August 13, 2024

Abstract

Solving very large linear systems of equations is a key computational task in science and technology. In many cases, the coefficient matrix of the linear system is rank-deficient, leading to systems that may be underdetermined, inconsistent, or both. In such cases, one generally seeks to compute the least squares solution that minimizes the residual of the problem, which can be further defined as the solution with smallest norm in cases where the coefficient matrix has a nontrivial nullspace. This work presents several new techniques for solving least squares problems involving coefficient matrices that are so large that they do not fit in main memory. The implementations include both CPU and GPU variants. All techniques rely on complete orthogonal decompositions that guarantee that both conditions of a least squares solution are met, regardless of the rank properties of the matrix. Specifically, they rely on the recently proposed “randUTV” algorithm that is particularly effective in strongly communication-constrained environments. A detailed precision and performance study reveals that the new methods, that operate on data stored on disk, are competitive with state-of-the-art methods that store all data in main memory.

Keywords: Numerical linear algebra, systems of linear equations, linear least-squares solutions, rank-revealing matrix factorization, high performance, blocked algorithm, algorithm-by-blocks.

1 Introduction

Let A be a matrix of dimension $m \times n$ and let b be a vector of dimension m . Let r denote the rank of the matrix to some given computational precision τ . In solving a linear system $Ax = b$, two complications may arise. If the rank r is smaller than m , it may be the case that the data vector b does not belong to the range of A , in which case the system is *inconsistent* since it does not admit an exact solution. If the rank r is smaller than n , then the matrix has a non-trivial nullspace, and the solution is not unique. When either or both complications are present, we generally look for the *least squares solution* x , which is defined by two conditions: (1) It minimizes the residual $\|Ax - b\|$ over $x \in \mathbb{R}^n$, and (2) among the minimizers, the solution x is the one with smallest magnitude. Different norms may be considered, but the Euclidean norm is the most common, and is the only one considered in this work.

In cases where the coefficient matrix has no nullspace (i.e. the matrix has full column rank), least squares problems may be solved very efficiently by using a plain (unpivoted) QR factorization [15] based on Householder transformations, which provide a good numerical stability.

However, for more general problems, state-of-the-art software is based on the singular value decomposition (SVD) [14], which ensures that both conditions of a least square solution are met, regardless of the aspect ratio and rank of the matrix. For computational efficiency, high-performance software often relies on *complete orthogonal decompositions* (CODs) [24], which generalize the SVD to build a decomposition of the form $A = UTV^*$, where U and V are unitary and T is triangular. Such decompositions can be

faster than the SVD, and are sufficient for computing the least square solution in a numerically stable way. One of the most practical methods for computing a COD is based on the column-pivoted QR factorization (CPQR), which requires a much lower computational cost than the SVD and usually reveals rank reasonably well. The original method was developed by Golub and Kahan, and was later optimized and refined for uncore architectures and shared-memory multicore/multiprocessor architectures [3, 35, 9]. Nevertheless, least squares solvers based on both SVD and CPQR are much slower than least-squares methods for full rank matrices based on the unpivoted QR factorization on current architectures because of the large ratio of matrix-vector operations of both the SVD and CPQR.

When working with matrices so large that they must be stored in an external device (also called stored Out-Of-Core or OOC), both least-squares solvers that employ the SVD and least-squares solvers that employ CPQR are strongly limited in performances because of the many slow matrix-vector operations required and the large amount of data being transferred. Some efforts for computing factorizations of dense OOC matrices include POOCLAPACK [17, 36, 16], the SOLAR library [42], a runtime to execute algorithms-by-blocks [32], as well as an OOC extension [7] to ScaLAPACK not included in this library. These efforts usually are limited to Cholesky, unpivoted QR, and LU decompositions. A truncated SVD algorithm that is effective for out-of-core matrices was introduced by Halko *et al.* [18]. This technique, however, only yields a *partial* factorization, and it requires upper bound for the target rank k known in advance. Recent works have been focused on computing the SVD of dense OOC matrices. Demchik *et al.* [8] employed randomization to compute the SVD, but no performance results for dense matrices were reported. Kabir *et al.* [25] used a two-stage approach for computing the SVD that reduces the dense matrix to band form in a first stage, which allowed to factorize matrices of up to dimension $100k \times 100k$.

In cases where the coefficient matrix is sparse but of high dimension, iterative techniques can be employed, such as LSQR [30], LSMR [11], LSMB [20], and other Krylov methods [37]. These methods have the advantage of iterating with the coefficient matrix without modifying it. Therefore, the required memory resources are lower, although the convergence rate can also be low. To accelerate convergence, they can be combined with preconditioners or regularization techniques [2, 12, 38, 39]. Recently, a method for computing preconditioners based on Krylov’s methods [4] was presented, and in most of the tests applying preconditioners accelerates the convergence of the iterative Krylov subspace method LSMR when having a rank-deficient problem.

Among the direct methods for sparse matrices, the QR approach is the most used, and there are several libraries that offer optimized methods, such as Intel’s MKL Sparse QR [10], SuiteSparse QR [13, 43], and the MUMPS QR solver [1]. Another option for large sparse systems is the Multilevel Incomplete QR preconditioning technique, included in the MIQR package [26]. However, all of them are focused on sparse matrices. If a part of the sparse matrix is dense, the factorization will fail if the main memory is not large enough. A recent work [40] proposes a hybrid approach to solve the problem if the matrix has some dense rows. Scott and Tuma divide the matrix into two parts: the sparse part and the dense part. They perform an updating, partial stretching or regularization on the matrix. Then, they use either the QR factorization or a hybrid QR-iterative method to solve the problem. This method is more robust and efficient, and the sparse part of the matrix can be rank deficient. Nevertheless, the main problem is that it is still proposed for mostly-sparse matrices, and memory resources may be insufficient when the problem is big enough or not sparse enough.

Some methods, such as the Pivoting Avoiding QR (PAQR) [41], can work with dense matrices as long as they fit in main memory. PAQR is a variant of the standard QR factorization that eliminates the need for explicit pivoting, making it a more efficient option for matrices with significant linear dependence. The key to the PAQR algorithm is the dynamic detection and elimination of linearly dependent columns during the factorization process. Instead of pivoting to remove dependent columns, PAQR identifies these columns and removes them directly from the process. This reduces the number of operations required and improves the performance of the algorithm, especially for matrices with a large number of linearly dependent columns. The results show that PAQR is significantly more efficient than QR for matrices with significant linear dependence.

However, in order to solve very large dense or not-so-sparse systems, other techniques must be employed. As nowadays disk space is much cheaper than main memory, an interesting approach is using Out-Of-Core techniques [17, 33].

The key contribution of the present manuscript is a set of algorithms and implementations for solving least squares problems via complete orthogonal decompositions when the coefficient matrix is too large to fit in main memory, and is instead stored “Out-Of-Core” (OOC) on cheaper disk space. Our work builds on prior least squares solvers for this environment that rely on the QR decomposition (making them suitable only for problems with full column rank) for both CPU and GPU architectures ([5] and [31],

respectively). The maximum matrix size assessed in those works was $266\,500 \times 262\,144$, which requires about 520 GB of storage when working with double-precision arithmetic, making it infeasible for methods that work with data in main memory (“in-core” computations) on most computers.

To enable the solution of least squares problems involving coefficient matrices of arbitrary sizes and arbitrary ranks, the QR factorization is swapped out in favor of the “randUTV” algorithm [28], which can be viewed as a blocked incremental version of the randomized SVD (RSVD) [19, 27]. The randUTV factorization can be implemented with high performances when data is stored Out-Of-Core on CPU architectures [22]. In our work, this randUTV implementation has been accelerated with some improvements, and then the technique is further extended to solve the linear least squares problem by incorporating the following three tasks: The first task is a simple rank estimation step. The second task is a computation that modifies the basis for the row space (encoded in the columns of V) so that it provides a clear split between the nullspace of the matrix and its orthogonal complement. This second task is necessary to ensure that a minimal norm solution is constructed. The third task is the final computations to obtain the solution x .

***Remark:** The manuscript also describes a version of the code that skips the second step, and relies instead on a direct truncation of the factorization resulting from the randUTV algorithm. This version computes a solution that minimizes the residual (up to floating-point precision), but is not guaranteed to result in a solution with minimal norm. However, since randUTV by itself is highly accurate in revealing the numerical rank, the loss of optimality is very minor, as demonstrated in several numerical examples.*

The main contributions of the manuscript are enumerated next:

- We present a new set of implementations for solving linear least-squares problems so large that they do not fit in main memory.
- Our new methods can solve linear systems with both full-rank and rank-deficient coefficient matrices, for both consistent and inconsistent problems.
- Our new methods work for any matrices that fit on the disk drive, regardless of whether they fit in main memory.
- Our work accelerates the speed of previous Out-Of-Core implementations of the randUTV factorization for CPU architectures by introducing several performance improvements. Moreover, we developed a new family of implementations for GPU architectures.
- A precision study of our new implementations has been performed, which includes both our own matrices and several large matrices from public repositories. The precision of the new codes is competitive with those of methods working in main memory.
- A thorough performance study has been performed. The performances of the new codes are competitive with those of state-of-the-art high-performance codes with similar functionality that work only on data stored in main memory (thus limited in size).
- The performances of our new codes are slower than those of specific methods for full-rank matrices, but only slightly so.
- Our new methods can be employed both in CPU architectures and GPU architectures, delivering good performance and precision in both cases.

The document is organized as follows: Section 2 describes the traditional algorithms for solving the linear least squares problem. Section 3 introduces our new approach for solving the linear least squares problem by using the randUTV factorization. Section 4 contains both a performance assessment and a precision study comparing our implementations with respect to high-performance implementations employed when the data fits in main memory. Finally, Section 5 enumerates the conclusions of our work.

2 Methods for Solving Linear Least-Squares Problems with Dense Coefficient Matrices

In this section, we briefly review the classical least squares problem and describe the principal algorithms for solving it. Throughout the section, A denotes a matrix of size $m \times n$, b denotes an $m \times 1$ vector, and we seek to solve the linear system

$$Ax = b$$

in a least squares sense. To be precise, we seek the x vector that satisfies the following two conditions:

- (1) The vector x minimizes the residual. In other words

$$\|Ax - b\| = \inf\{\|Ay - b\| : y \in \mathbb{R}^n\}.$$

- (2) If the problem in (1) has more than one solution, then x is the solution with minimal norm.

Throughout the manuscript, $\|\cdot\|$ denotes Euclidean norm, unless otherwise noted.

2.1 Methods based on the unpivoted QR decomposition

When A has full column rank (so that $\text{rank}(A) = n$), condition (2) is not operable, and the least squares solution can be computed via an unpivoted QR decomposition. In this case, the first step is to build the factorization $A = QR$, where $Q \in \mathbb{R}^{m \times n}$ has orthonormal columns and $R \in \mathbb{R}^{n \times n}$ is upper triangular. The least squares solution is then $x = R^{-1}(Q^*b)$. Note that since R is triangular, there is no need to compute the explicit inverse of R . Also note that the matrix Q does not need to be explicitly built, and can be applied to b on-the-fly when factorizing the matrix A .

2.2 Methods based on the singular value decomposition

In the case where the coefficient matrix does not have full column rank, the standard tool for solving the least squares problem is based on truncating the singular value decomposition (SVD). In this approach, one first computes a factorization $A = U\Sigma V^*$, where U and V are unitary and Σ is diagonal. The next step is to determine the numerical rank r of the matrix to some given tolerance τ , and partition the factors so that

$$A = \begin{bmatrix} U_1 & U_2 \end{bmatrix} \begin{bmatrix} \Sigma_{11} & 0 \\ 0 & 0 \end{bmatrix} \begin{bmatrix} V_1^* \\ V_2^* \end{bmatrix},$$

where Σ_{11} is of size $r \times r$. The least squares solution is finally $x = V_1 \Sigma_{11}^{-1} (U_1^* b)$.

2.3 Methods based on complete orthogonal decompositions

Techniques based on the SVD form the gold standard for solving least squares problems. Due to the high cost of computing a full SVD, a simplified procedure based on complete orthogonal decompositions (CODs) is sometimes used. The idea is to form a factorization $A = UTV^*$, where U and V are unitary and T is triangular. Concretely, the SVD is a special case of a COD, and the reason to introduce additional flexibility in the middle factor is that it enables simpler and faster algorithms.

The standard approach for computing a COD is via two orthogonal factorizations. The first one computes $AV = UT$, where V is a permutation matrix, U is unitary, and T is upper triangular. The rank r is detected as the number of non-zero rows in T , so that the factorization takes the form

$$AV = \begin{bmatrix} U_1 & U_2 \end{bmatrix} \begin{bmatrix} T_{11} & T_{12} \\ 0 & 0 \end{bmatrix} = U_1 [T_{11}, T_{12}],$$

where T_{11} is of size $r \times r$.

Then, a second orthogonal factorization is used to build an orthonormal basis for the row space of A through a factorization $[T_{11}, T_{12}] = S_{11}^* W^*$, where $W \in \mathbb{R}^{n \times r}$ has orthonormal columns and $S_{11} \in \mathbb{R}^{r \times r}$ is upper triangular. In other words, we build the factorization $AV = U_1 S_{11}^* W^*$. The least square solution is then $x = V W (S_{11}^*)^{-1} (U_1^* b)$. Note that in practice the matrix A is typically rank deficient only to some preset tolerance τ .

3 Solving the linear least-squares problem with the randUTV factorization

The methods we propose follow the traditional template of methods based on complete orthogonal decompositions described in Subsection 2.3. The key difference is that the first step of our process uses the ‘‘randUTV’’ algorithm, which given a matrix $A \in \mathbb{R}^{m \times n}$ computes a decomposition

$$\begin{matrix} A & V & = & U & T & , \\ m \times n & n \times n & & m \times m & m \times n & \end{matrix} \quad (1)$$

where U and V are unitary, and T is upper triangular. The key difference to the traditional techniques is that we allow V to involve unitary transformations beyond column permutations. This additional freedom has two benefits: The first one is that it allows the algorithm to be *blocked*, which is essential for high-performance Out-Of-Core implementations like the one described here. The second one is that it allows for much stronger rank-revealing properties, in the sense that most of the mass of T gets moved to the diagonal, with off-diagonal entries being much smaller in magnitude than in column-pivoted QR (CPQR). This second benefit is important in the present context since it allows us to estimate the numerical rank with a higher accuracy.

In this section, we briefly review randUTV, and then describe the details of how we implement it in the present context.

3.1 The randUTV algorithm

The randUTV algorithm takes as its input a general matrix $A \in \mathbb{R}^{m \times n}$ and a block size n_b , and drives A to upper triangular form via a sequence of $s = \lceil n/n_b \rceil$ unitary transformations. (We refer to the matrix T as “upper triangular” even in the case $n < m$, where T is technically “trapezoidal”.) We start with $T^{(0)} := A$. In the i -th iteration ($i = 1, 2, \dots, s$), a matrix $T^{(i)} \in \mathbb{R}^{m \times n}$ is formed by the computation

$$T^{(i)} := \left(U^{(i)} \right)^* T^{(i-1)} V^{(i)}, \quad (2)$$

where $U^{(i)} \in \mathbb{R}^{m \times m}$ and $V^{(i)} \in \mathbb{R}^{n \times n}$ are unitary matrices chosen to introduce zeros under the diagonal of the matrix, and to promote the rank-revealing quality of the decomposition. Figure 1 shows the general pattern of the transformations for a toy example.

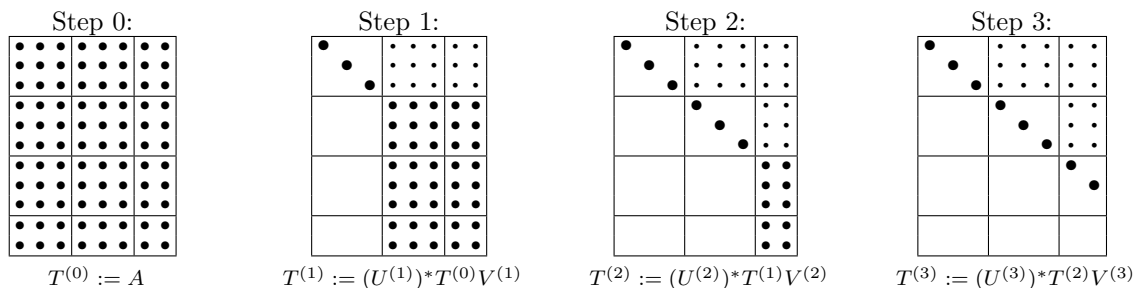


Figure 1: The sparsity patterns of the four matrices $T^{(i)}$ that appear in randUTV, shown for the particular case where $m = 11, n = 8$, and $n_b = 3$. The size of each element is a rough approximation of its absolute value.

The theoretically ideal UTV decomposition is one where the first j columns of U/V span the same space as the dominant j left/right singular vectors of A . The randUTV algorithm gets close to this optimum through a randomized subspace approximation that proceeds in blocks of n_b vectors. To be precise, in the first step of randUTV, a matrix $G \in \mathbb{R}^{m \times n_b}$ is drawn from a Gaussian distribution, and a sample matrix $Y = A^*G$ is computed. The first n_b columns of V are then constructed to form an orthonormal (ON) basis for the space spanned by the columns of Y , and the first n_b columns of U are constructed to form an ON basis for the space spanned by the columns of $AV(:, 1 : n_b)$. The block $T(1 : n_b, 1 : n_b)$ is diagonal, and holds the n_b singular values of $Y = A^*G$.

To further strengthen the rank revealing properties of randUTV, a small number of power iterations can be incorporated into the randomized sampling, so that we instead build the sample matrix $Y = (A^*A)^q A^*G$ for some small integer q . In practice, $q = 1$ or $q = 2$ is sufficient to yield very high accuracy (the diagonals approximate the singular values with several digits of precision).

Once the first step of randUTV has been completed, the first n_b columns of the initial matrix $T^{(0)} = A$ have been driven to upper triangular form in the updated matrix $T^{(1)} = (U^{(1)})^* T^{(0)} V^{(1)}$. The process is then repeated on the matrix formed by excluding the first n_b columns and rows of $T^{(1)}$, and continues through a sequence of unitary transforms until an upper triangular matrix has been obtained.

Figure 2 shows the complete randUTV algorithm written with the FLAME methodology/notation. In this algorithm, the second output argument of the unpivoted QR factorization is the upper triangular factor, whereas the third one is the unit lower trapezoidal matrix with the Householder vectors.

Remark 1 (Connection to randomized SVD) *The randUTV algorithm can be viewed as a blocked and incremental version of the randomized SVD (RSVD) algorithm of [27, 29, 19]. To be precise, the*

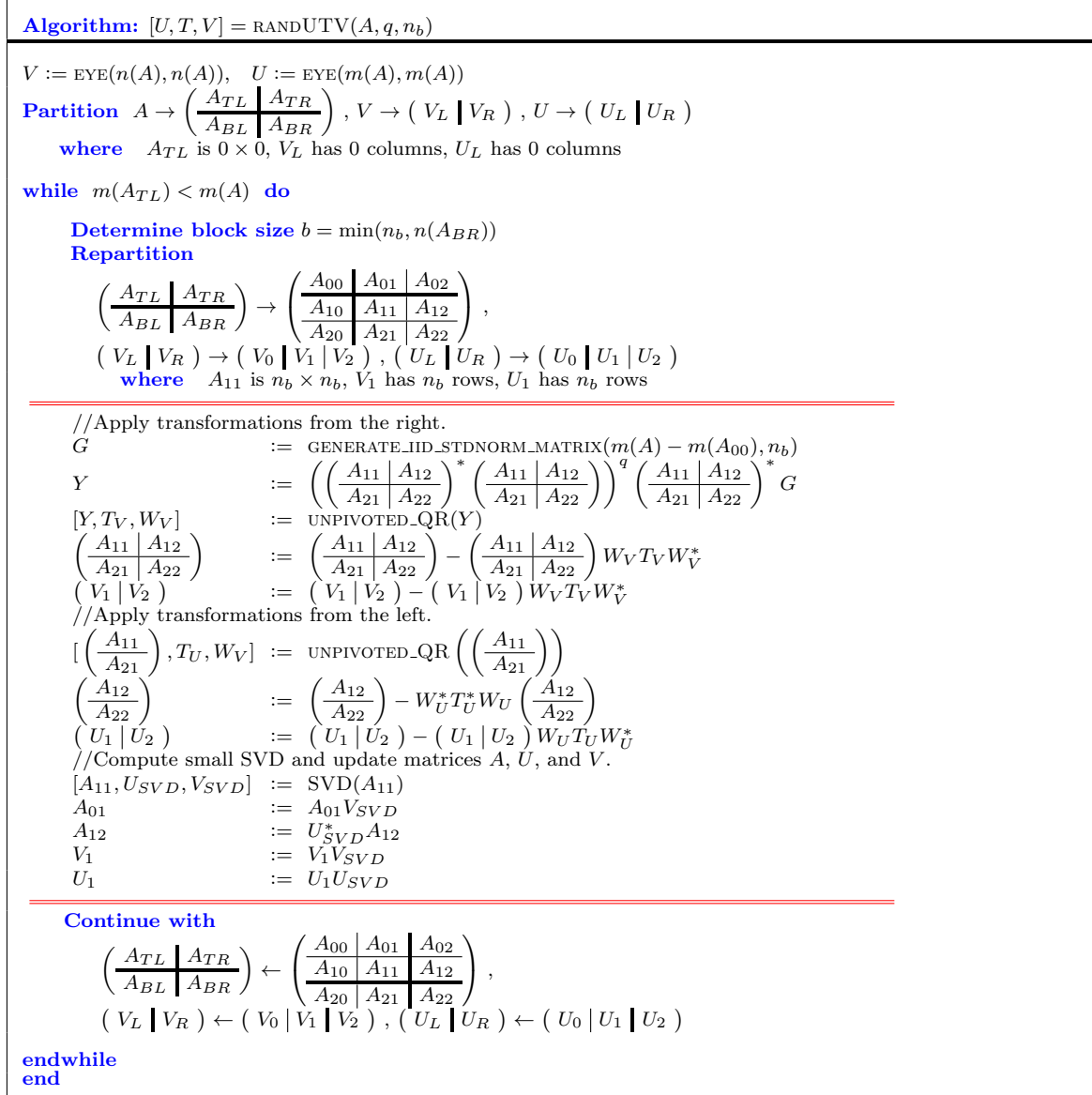


Figure 2: The randUTV algorithm written with the FLAME methodology/notation.

matrix

$$U(:, 1 : n_b) T(1 : n_b, 1 : n_b) (V(:, 1 : n_b))^*$$

is exactly the rank n_b approximation to A generated by the RSVD, as described in [19, Sec. 1.6] (without “over sampling”).

Our description of randUTV was purposefully kept brief in this section, as it has been described in detail in a sequence of recent papers. The original paper [28] contains a detailed discussion of its rank revealing properties, with numerical experiments that demonstrate that in practice it gets very close to the optimality of the SVD. Details on implementing it in different computational environments can be found in [22, 23, 21].

3.2 Adapting randUTV to solve the least squares problem

When the matrix A does not possess a nullspace, the factorization in Eq. 1 can be used directly to compute the least squares solution of $Ax = b$ through the formula

$$x = VT(1 : n, 1 : n)^{-1} U(1 : n, :)^* b. \quad (3)$$

In the cases where there is a non-trivial nullspace, some additional work may be required to ensure that both conditions for a least squares solution are satisfied. In this case, the computed UTV factorization

takes the form

$$\begin{array}{ccc} A & = & U_1 \begin{bmatrix} T_{11} & T_{12} \end{bmatrix} V^* \\ m \times n & & m \times r \quad r \times n \quad n \times n \end{array}, \quad (4)$$

where r is the rank of the matrix and $T_{11} \in \mathbb{R}^{r \times r}$ is upper triangular. (In practice, the rank will typically be estimated by considering diagonal entries of T below some given threshold τ to be zero, in which case (4) holds only approximately.) One could now immediately build the solution

$$x_{\text{simple}} = V(:, 1:r) T_{11}^{-1} U_1^* b, \quad (5)$$

which would be guaranteed to satisfy the first condition of least squares solution (i.e. that $\|Ax_{\text{simple}} - b\| = \inf_y \|Ay - b\|$). However, x_{simple} is not necessarily the minimal norm solution among the minimizers. To ensure that both conditions are satisfied, our software performs by default an additional orthogonal factorization of the matrix $[T_{11}, T_{12}]$, as described in Section 2.3, and conforming to the xGELSY functions in LAPACK [34].

Figure 3 shows the algorithm for nullifying T_{12} written with the FLAME methodology/notation. The input arguments are the following: T is the upper triangular factor of the randUTV factorization of A , V is the right orthogonal matrix of the randUTV factorization, and r is the numeric rank of T . Matrices C , D , E , and F are views of the original matrices: Changes made to them are also made to the original matrices.

Algorithm: $[T, V] = \text{NULLIFY_TOP_RIGHT_PART_OF_T}(T, V, r)$

$\left(\begin{array}{c|c} C & D \\ * & * \end{array} \right) := T$, where C is $r \times r$, D is $r \times (n - r)$,
 $\left(\begin{array}{c|c} E & F \end{array} \right) := V$, where E is $n \times r$, F is $n \times (n - r)$

Partition $C \rightarrow \left(\begin{array}{c|c} C_{TL} & C_{TR} \\ C_{BL} & C_{BR} \end{array} \right)$, $D \rightarrow \left(\begin{array}{c} D_T \\ D_B \end{array} \right)$, $E \rightarrow (E_L \mid E_R)$
where C_{BR} is 0×0 , D_B has 0 rows, E_R has 0 columns

while $m(C_{BR}) < m(C)$ **do**

Repartition

$\left(\begin{array}{c|c} C_{TL} & C_{TR} \\ C_{BL} & C_{BR} \end{array} \right) \rightarrow \left(\begin{array}{c|c|c} C_{00} & C_{01} & C_{02} \\ C_{10} & C_{11} & C_{12} \\ C_{20} & C_{21} & C_{22} \end{array} \right)$, $\left(\begin{array}{c} D_T \\ D_B \end{array} \right) \rightarrow \left(\begin{array}{c} D_0 \\ D_1 \\ D_2 \end{array} \right)$,
 $(E_L \mid E_R) \rightarrow (E_0 \mid E_1 \mid E_2)$
where C_{11} is $b \times b$, D_1 has b rows, E_1 has b columns

$[C_{11}, D_1] := \text{NULLIFY}(C_{11}, D_1)$
 $[C_{01}, D_0] := \text{UPDATE}(C_{11}, D_1, C_{01}, D_0)$
 $[E_1, F] := \text{UPDATE}(C_{11}, D_1, E_1, F)$

Continue with

$\left(\begin{array}{c|c} C_{TL} & C_{TR} \\ C_{BL} & C_{BR} \end{array} \right) \leftarrow \left(\begin{array}{c|c|c} C_{00} & C_{01} & C_{02} \\ C_{10} & C_{11} & C_{12} \\ C_{20} & C_{21} & C_{22} \end{array} \right)$, $\left(\begin{array}{c} D_T \\ D_B \end{array} \right) \leftarrow \left(\begin{array}{c} D_0 \\ D_1 \\ D_2 \end{array} \right)$,
 $(E_L \mid E_R) \leftarrow (E_0 \mid E_1 \mid E_2)$

endwhile
end

Figure 3: The algorithm to nullify the top right part of T written with the FLAME methodology/notation. The input arguments are the following: T is the upper triangular factor of the randUTV factorization of A , V is the right orthogonal matrix of the randUTV factorization, and r is the numeric rank of T .

Figure 4 shows the overall algorithm algorithm for solving $Ax = b$ written with the FLAME methodology/notation.

Remark 2 (Fast option) *Due to the fact that randUTV is very precise in revealing the numerical rank, the extra orthonormalization step can in fact be dropped with minimal impact on the norm of the residual. Our software offers this “accelerated version” as an option for users who do not need a guarantee that the absolute minimal norm solution is returned.*

3.3 Blocked implementation for In-Core data

When solving linear systems with orthogonal transformations, the most-common computational tasks are the computation of a Householder transformation and its application to some matrix columns (or

```

Algorithm:  $[x] = \text{SOLVE\_LINEAR\_SYSTEM}(A, b, q)$ 

 $[U, T, V] := \text{RANDUTV}(A, q, n_b)$ 
 $[r] := \text{COMPUTE\_RANK}(T)$ 
 $[T, V] := \text{NULLIFY\_TOP\_RIGHT\_PART\_OF\_T}(T, V, r)$ 
 $[x] := V(T_{ll}^{-1}(U^*b))$ , where  $T_{ll} = T(1:r, 1:r)$ 
end

```

Figure 4: The overall algorithm for solving $Ax = b$. The input arguments are the following: A is the coefficient matrix of dimension $m \times n$, b is the independent vector of dimension $m \times 1$, and q is the number of steps in the power iteration process.

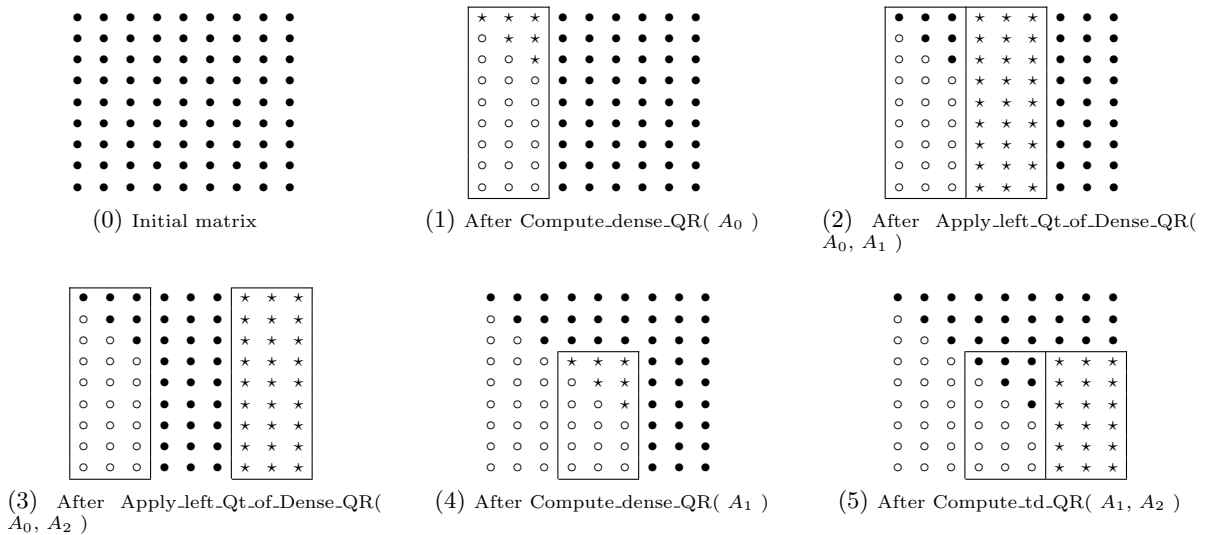


Figure 5: An illustration of the first tasks performed by a blocked algorithm for computing the QR factorization. The ‘●’ symbol represents an element not modified by the current task, ‘★’ represents an element modified by the current task, and ‘○’ represents a nullified element. The continuous lines surround the blocks involved in the current task.

rows). Scalar algorithms apply these transformations one by one to the rest of the matrix (right-looking algorithms) or to the current column (left-looking algorithms). To apply one Householder transformation to the rest of the matrix, all the rest of the matrix must be read into the CPU, which requires a lot of memory accesses.

In contrast, blocked algorithms apply several Householder transformations at the same time, thus reducing the amount of data being transferred between main memory and the CPU. Moreover, they allow the use of highly-efficient matrix-matrix operations, which perform many floating-point operations per memory access (high arithmetic intensity), which is key to obtain high performances.

Figure 5 shows a graphical representation of a blocked algorithm for computing the QR factorization with a right-looking algorithm (others factorizations would be similar). For the sake of brevity, this figure shows only its first tasks. In this figure, the ‘★’ symbol represents an element modified by the current task. The ‘○’ symbol represents an element that has been nullified. Note that ‘○’ elements do not actually store zeros but information about the Householder transformations that will be later used to apply them. The continuous lines surround the blocks involved (read or written) in the current task.

Martinsson *et al.* [28] developed a blocked algorithm for computing the randUTV. The experimental study showed that their implementation was competitive with high-performance implementations of both the SVD and CPQR from the Intel MKL library. Although the randUTV requires many more floating-point operations than the other two factorizations (CPQR and SVD), most of those floating-point operations are done inside BLAS-3 subroutines (matrix-matrix operations), which yields a high computational speed.

3.4 Algorithm-by-blocks implementation for In-Core data

Although obtaining higher performances than scalar algorithms, blocked algorithms usually contain a performance bottleneck. The applying of the transformations to the rest of matrix is usually very efficient:

BLAS-3 operations can be applied and all cores are usually busy doing work. On the other side, the computation of the transformations usually involve only a small number of columns with only a small amount of floating-point operations, and during these, only one core is busy and the rest of cores are idle, which can greatly decrease performances when having many cores.

To overcome this problem, algorithms-by-blocks work in a different way. They apply the traditional algorithm on square blocks instead of scalars, and hence the name. The original scalar algorithm is converted on a series of tasks, where every task operates on a few blocks (usually two, three, or four). Figure 6 shows a graphical representation of a right-looking variant of an algorithm-by-blocks for computing a QR factorization. For the sake of brevity, this figure shows only its first tasks. In this figure, blocks involved in the current task are in bold face, blocks modified by the current task are marked with the ‘*’ superscript, and blocks nullified are marked with the ‘0’ symbol. Note that nullified blocks do not actually store zeros but information about the Householder transformations that will be later used to apply them.

$$\begin{array}{ccc}
\left(\begin{array}{c|c|c} A_{00} & A_{01} & A_{02} \\ \hline A_{10} & A_{11} & A_{12} \\ \hline A_{20} & A_{21} & A_{22} \end{array} \right) & \left(\begin{array}{c|c|c} \mathbf{A}_{00}^* & A_{01} & A_{02} \\ \hline A_{10} & A_{11} & A_{12} \\ \hline A_{20} & A_{21} & A_{22} \end{array} \right) & \left(\begin{array}{c|c|c} \mathbf{A}_{00} & \mathbf{A}_{01}^* & A_{02} \\ \hline A_{10} & A_{11} & A_{12} \\ \hline A_{20} & A_{21} & A_{22} \end{array} \right) \\
(0) \text{ Initial matrix} & (1) \text{ After Compute_dense_QR}(A_{00}) & (2) \text{ After Apply_left_Qt_of_Dense_QR}(A_{00}, A_{01}) \\
\\
\left(\begin{array}{c|c|c} \mathbf{A}_{00} & A_{01} & \mathbf{A}_{02}^* \\ \hline A_{10} & A_{11} & A_{12} \\ \hline A_{20} & A_{21} & A_{22} \end{array} \right) & \left(\begin{array}{c|c|c} \mathbf{A}_{00}^* & A_{01} & A_{02} \\ \hline \mathbf{0}^* & A_{11} & A_{12} \\ \hline A_{20} & A_{21} & A_{22} \end{array} \right) & \left(\begin{array}{c|c|c} \mathbf{A}_{00} & \mathbf{A}_{01}^* & A_{02} \\ \hline \mathbf{0} & \mathbf{A}_{11}^* & A_{12} \\ \hline A_{20} & A_{21} & A_{22} \end{array} \right) \\
(3) \text{ After Apply_left_Qt_of_Dense_QR}(A_{00}, A_{02}) & (4) \text{ After Compute_td_QR}(A_{00}, A_{10}) & (5) \text{ After Apply_left_Qt_of_td_QR}(A_{00}, A_{10}, A_{01}, A_{11}) \\
\\
\left(\begin{array}{c|c|c} \mathbf{A}_{00} & A_{01} & \mathbf{A}_{02}^* \\ \hline \mathbf{0} & A_{11} & \mathbf{A}_{12}^* \\ \hline A_{20} & A_{21} & A_{22} \end{array} \right) & \left(\begin{array}{c|c|c} \mathbf{A}_{00}^* & A_{01} & A_{02} \\ \hline 0 & A_{11} & A_{12} \\ \hline \mathbf{0}^* & A_{21} & A_{22} \end{array} \right) & \left(\begin{array}{c|c|c} \mathbf{A}_{00} & \mathbf{A}_{01}^* & A_{02} \\ \hline 0 & A_{11} & A_{12} \\ \hline \mathbf{0} & \mathbf{A}_{21}^* & A_{22} \end{array} \right) \\
(6) \text{ After Apply_left_Qt_of_td_QR}(A_{00}, A_{10}, A_{02}, A_{12}) & (7) \text{ After Compute_td_QR}(A_{00}, A_{20}) & (8) \text{ After Apply_left_Qt_of_td_QR}(A_{00}, A_{20}, A_{01}, A_{21})
\end{array}$$

Figure 6: An illustration of the first tasks performed by an algorithm-by-blocks for computing the QR factorization. Blocks involved in the current task are in bold face, blocks modified by the current task are marked with the ‘*’ superscript, and blocks nullified are marked with the ‘0’ symbol.

Like blocked algorithms, algorithms-by-blocks also reduce the amount of data transferred and allow to use BLAS-3 subroutines. In this case, BLAS-3 subroutines are used inside each task. Another advantage is that many tasks on blocks can be performed in parallel. For instance, in the previous figure, tasks in subfigures 2 and 3 can be simultaneously executed. Moreover, tasks in subfigures 2, 3, and 4 could be simultaneously executed if a copy of the Householder transformations in A_{00} was done before. The main advantage of algorithm-by-blocks is that they do not contain parts with strong bottlenecks in which only one core can work and the remaining ones are idle. In this type of algorithms, several tasks can be usually performed in parallel. And even if one task could not be overlapped, its computational cost would be small (since all the operands are $n_b \times n_b$), and hence the bottleneck would be small too. In contrast, blocked algorithms usually have larger bottlenecks. For instance, in the blocked column-oriented right-looking algorithm for computing the QR factorization, the bottleneck is the factorization of the current column block, which can be up to $m \times n_b$.

Heavner *et al.* [21] developed and assessed an algorithm-by-blocks for computing the randUTV factorization on shared-memory multicore and multiprocessor architectures. Their implementations of the algorithm-by-blocks for computing the randUTV factorization can be more than twice as fast as the implementations of the blocked algorithms for the same computation. That work also shows that despite performing between 3.5 ($q = 0$) about 5.5 ($q = 2$) as many floating-point operations as the CPQR, it is several times faster than it (because of being very rich in BLAS-3 operations, as previously told). Moreover, it is also faster than a very high-performance implementation of the SVD factorization included in Intel MKL.

3.5 Out-Of-Core implementations for the least-squares problem with the randUTV

In some problems, the data to be processed is much larger than the available main memory in the computer. In these cases, there are several options. The first one is to acquire a computer with a main memory so large that the data fits inside it. The second one is to use a distributed-memory architecture with multiple nodes so that the total main memory is larger, which requires several nodes (computers) and a high-speed communication network to connect them. In either case, the cost is much higher and in some cases it could be beyond affordable.

A different option is to rewrite the software so that not all of the data is stored in main memory all of the time. By rewriting the software, affordable computers already acquired or newly acquired affordable computers can be employed.

The traditional technique is to decompose the work to do into several computational major tasks. Then, for every task, the data to be used must be loaded from secondary storage (disk) to main memory, then processed there, and finally the data modified must be copied back from main memory to secondary storage. Blocked algorithms can employ this pattern. For instance, in a right-looking algorithm for computing the QR factorization, a block of columns is loaded, then factorized, and finally written back into disk storage. Then, the rest of the matrix must be updated also by blocks of columns. That is, a block of columns of the rest of the matrix is loaded, then modified, and then written back into disk. See Figure 5 again for a graphical representation of a blocked algorithm for computing a factorization.

However, as can be easily seen in this figure, when applying this technique, the amount of data being transferred and processed is smaller in each iteration. For instance, compare the amount of data transferred and processed in the first iteration (subfigures 1, 2, and 3) and in the second iteration (subfigures 4 and 5). The problem with this approach is that after each iteration of the blocked algorithm, main memory is taken advantage less and less. In the final iterations of the blocked algorithm, only a small amount of the main memory is used. If we want to take advantage of most of main memory in the first iteration, we must adjust the block size according to the main memory size and to the number of rows m . And that only guarantees maximum usage of main memory in the first iteration.

In contrast, algorithm-by-blocks can also match the pattern of loading the data to be used from secondary storage (disk) to main memory, then process it, and finally copy back the data modified from main memory into secondary storage. In this case, in order to take full advantage of main memory, the block size does not depend on m and n (the dimensions of matrix A) at all. The amount of data transferred and processed does not decrease as the algorithm iteration advances, and it depends only on the type of task being executed.

Heavner *et al.* [22] developed an Out-Of-Core implementation of the randUTV factorization attaining high performance for CPU architectures.

In our work, we have applied some performance improvements to this previous implementation of the randUTV factorization for CPU architectures: The use of broader (more complex) computational kernels and the implementation of a new block cache management policy. Moreover, we have developed a new family of implementations for GPU architectures. This implementation is further refined to solve the linear least squares problem by incorporating the additional three tasks: The first one is a simple rank estimation step. The second one is the annihilation of the top right block of dimension $r \times (n - r)$ of T to provide a clear split between the nullspace of the matrix and its orthogonal complement. The third task is the final computations to obtain the solution x .

3.5.1 New implementations

In this work we present several implementations for solving the linear least squares problem with rank-deficient (or full-rank) coefficient matrices by using the randUTV factorization. For a better performance analysis (by isolating every technique), each one of the following variants usually contributes a specific improvement with respect to the previous one. The variants for CPU architectures are described next:

- **v21t**: This is a straightforward implementation for solving rank-deficient linear systems by using the randUTV factorization on CPU multicore systems. In this case both matrices U and V are explicitly built. This is the traditional Out-Of-Core implementation: In order to perform every task, all the input operands are brought from disk to main memory, then they are processed, and finally the output operands are written back to disk.
- **v22t**: As said, this is a modification of the previous one **v21t**. Previous variant **v21t** is implemented with the traditional approach of using BLAS-3 subroutines (**dgemm**, **dtrsm**, etc.) from a high-

performance BLAS library such as the Intel MKL library since it usually renders high performance gains. In contrast, the `v22t` variant employs broader (more complex) computational methods (`dlarfb`, `dgeqrf`, `dormqr`, etc.) from the same library since they have been greatly optimized by this company.

- `v23t`: Modification of `v22t`. In this variant, matrix U is not explicitly built, and the left orthogonal transformations are applied to b (or B) on-the-fly. The main advantage is that a lot of computation and data transfers can be saved since the full matrix U is not computed, thus obtaining higher performances. In this case, we can solve as many linear systems (as many columns in B) as desired. On the other hand, if this approach is used, the `randUTV` factorization cannot be later reused to solve other linear systems with a different matrix B .
- `v23c`: Modification of `v23t`. It employs a block cache with the aim of saving transfers of operands between main memory and disk. For instance, if two consecutive tasks are the following: `Compute_dense_QR(A00)` and `Apply_dense_QR(A00, A01)`, then the traditional approach loads operand A_{00} , processes it, and then stores it. Then, to process the second task, the operand A_{00} must be loaded again. By using a cache of blocks stored in main memory, the second load of A_{00} can be saved, thus reducing the amount of data transfers between main memory and disk.

To accelerate the cache management, all slots in the block cache are created with the maximum square block size. It also employs a four-set associative method (a block can only be stored in one of the four sets) to reduce the block search. The eviction cache policy to discard blocks when the cache is full (and no other block can be brought) is the LRU (Least-Recently Used) policy, since it usually renders good results.

- `v23d`: Modification of `v23c`. It employs a block cache with the same LRU (Least-Recently Used) policy. This variant introduces two improvements with respect to the previous one: The first one is that the slots in the block cache are of the same size of the blocks actually stored. The second one is that a block can be stored in any position (no four-set associative method). The first change allows to fit more blocks in the cache, but requires a more complex management. The second change allows a block to be stored in any gap, but can make the block search slower.
- `v23e`: Modification of `v23d`. The LRU policy for cache replacement offers usually good results (a good hit/miss ratio) since it tries to reduce the number of cache misses by using the past behavior to foresee the next data transfers. In our case, since the list of tasks has been already completely built before the execution starts, it can effectively be used to choose the block to be replaced. In this case, we have decided to use the LFU (Latest in the Future to be Used) eviction policy. When having to discard one block, the block chosen to be discarded is the block being used latest in the future, which guarantees a very good hit/miss ratio.
- `v23x`: Modification of `v23e`. In this case, the overlapping of computation and disk I/O is employed to improve performances again. To achieve this, the implementations use two threads: the disk I/O thread and the computational thread. The disk I/O thread manages all the I/O of the program and the block cache. When processing tasks, it tries to stay ahead of the computational thread so that all operands are ready when the computational thread wants to execute a task. To do that, the disk I/O thread must bring operands in advance, and then it must write back operands when the cache is full. The computational thread executes the tasks if the operands are ready. If the operands are not ready, the computational thread must wait. In this case, both threads work according to the producer-consumer pattern.
- `v23s`: Modification of `v23x`. Unlike the previous one, this variant uses page-locked memory (*pinned* memory) for the whole block cache. The page-locked memory is a user-defined part of the main memory that the operating system cannot move to disk when the operating system has virtual memory and there is not enough main memory to store all the programs and data. This can accelerate some accesses because this part of the memory cannot ever be chosen to be moved into the disk by the operating system. In the case of CPU variants, the page-locked memory is asked to the operating system with one system call.
- `v24s`: Modification of `v23s`. This variant does not annihilate block T_{12} after computing the `randUTV` factorization, since the norm of this block is usually small after this factorization. Recall that block T_{12} is the top right block of the computed factor T with dimension $r \times (n - r)$, where r and n are the numerical rank and the number of columns of matrix A , respectively.

The variants for GPU architectures are described next. In this case, this number is smaller since we have used the insights of CPU variants to reduce them (as well as the number of experiments). In the case of GPU variants, we have used the C programming language and the cuSOLVER and cuBLAS libraries.

- **v33t**: Migration of **v23t** for GPU systems.
- **v33c**: Migration of **v23c** for GPU systems.
- **v33d**: Migration of **v23d** for GPU systems.
- **v33e**: Migration of **v23e** for GPU systems.
- **v33x**: Migration of **v23x** for GPU systems.
- **v33s**: Migration of **v23s** for GPU systems. In this variant the page-locked memory is asked to the NVIDIA driver as performances are better than when asked to the operating system. The page-locked memory is managed by the operating system, but asking to the NVIDIA driver helped it to be much more aware of it.
- **v34s**: Migration of **v24s** for GPU systems.

4 Numerical analysis

In this section, we investigate the numerical behavior of the new Out-Of-Core implementations for solving the linear least-squares problem and compare it with current high-performance implementations that work with data stored in main memory. First, the precision of the implementations is assessed; then, the performances are assessed. In all the experiments, double-precision real matrices were processed.

4.1 Precision analysis

This subsection contains an analysis of the precision obtained when solving the least-squares problem using different scenarios.

In a preliminary precision analysis we compared all of our new implementations for solving the linear least-squares problem. The results showed that all of them obtained similar results. For the sake of brevity, in the rest of this subsection we only report two variants, **v33s** and **v34s**, since their approach is very different: The first one employs the usual complete method, whereas the second one skips the annihilation of T_{12} .

In all the precision experiments, we have used $q = 0$ (number of steps in the power iteration process), since this number has been usually enough to reveal the rank with accuracy. If a good approximation to the singular values were required, then this number should be larger (usually $q = 1$ and $q = 2$ deliver good approximations of up to several digits to the singular values).

To be used as a reference, we also assessed two currently widely used implementations that work on main memory (in-core):

- **MKL.GELSS**: The linear least-squares solver **dGELSS** from the Intel MKL library. This implementation is based on the SVD (see Subsection 2.2).
- **MKL.GELSY**: The linear least-squares solver **dGELSY** from the Intel MKL library. This implementation is based on a complete orthogonal decomposition based on the column-pivoting QR factorization (see Subsection 2.3).

The platform employed to assess the precision was **aurus**. It is a server with two AMD EPYC 7282 processors (32 cores in total) at a base clock frequency of 2.8 GHz and 512 GiB of RAM. This server also has an NVIDIA A100 GPU with 80 GiB of RAM. The operating system is Rocky Linux 8.7. The C compiler is GNU gcc 8.5.0 20210514 (Red Hat 8.5.0-16). The computational libraries employed are Intel oneAPI Math Kernel Library Version 2023.1-Product Build 20230303 and Nvidia CUDA 11.7.

Matrix	m	n	nnz	rank
162bit	3,606	3,597	37,118	3,460
176bit	7,441	7,431	82,270	7,110
192bit	13,691	13,682	154,303	13,006
208bit	24,430	24,421	299,756	22,981
Maragal_6	21,255	10,152	537,692	8,331
Maragal_7	46,845	26,564	1,200,537	20,843

Table 1: Selected test matrices for the precision analysis.

4.1.1 Test matrices

In order to assess the precision, a set of test matrices from the Suite Sparse Matrix Collection [6] were selected. Table 1 shows the main features of their coefficient matrices. Note that all of them are rank-deficient. When the precision of some other methods on those problems was reported in other works, we included their results here.

In addition to the coefficient matrices A , this matrix suite sometimes provides vectors b . If the problem provides a right-hand side vector b , it is used. If not provided, three additional different types of vectors b were generated. Next, we describe the four different scenarios assessed:

- Scenario 1: Vector b is provided in the Suite Sparse Matrix Collection.
- Scenario 2: Vector b is set to ones. In this case, the system $Ax = b$ does not have a known solution.
- Scenario 3: Vector b is generated as $b = Ax$, where x is generated randomly.
- Scenario 4: Vector b is generated as $b = Ax$, where x is generated randomly. Additionally, b is slightly perturbed.

4.1.2 Scenario 1: Vector b is provided

Unfortunately, only two problems in the Suite Sparse Matrix Collection included vector b : Maragal_6 and Maragal_7. Table 2 shows the residuals obtained in these problems. As can be easily seen, the residuals are the same for all methods.

Matrix	Method			
	v33s	v34s	MKL_GELSS	MKL_GELSY
Maragal_6	4.53e-04	4.53e-04	4.53e-04	4.53e-04
Maragal_7	3.71e-06	3.71e-06	3.71e-06	3.71e-06

Table 2: Residuals $\|Ax - b\|_F$ when b is provided.

Scott [38] solved these problems by using the iterative method LSMR based on a Cholesky-based preconditioner that modifies the diagonal of the unregularized matrix to obtain matrices that are easier to factorize. The residuals for the Maragal_6 and Maragal_7 problems obtained by that work are 1.069e+01 and 1.369e+01, respectively, much higher than those obtained by both our implementations and the reference implementations.

Table 3 shows the norm of the solutions x . Recall that v33s performs the complete process, whereas v34s skips the annihilation of T_{12} . As can be seen in the table, the norm in each case is the same for both variants, and nearly equal to the norm of the solution obtained by the MKL methods.

Matrix	Method			
	v33s	v34s	MKL_GELSS	MKL_GELSY
Maragal_6	1.00e+01	1.00e+01	9.83e+00	9.83e+00
Maragal_7	1.96e+01	1.96e+01	1.81e+01	1.81e+01

Table 3: Norm of the solution $\|x\|_F$ when b is provided.

4.1.3 Scenario 2: Vector b is set to ones

In this scenario, vector b was set to ones. Hence, the system does not have a known solution. Table 4 shows the residuals of the solution for every test matrix. As can be seen, the residuals of the four methods were the same with three digits of precision.

Matrix	Method			
	v33s	v34s	MKL_GELSS	MKL_GELSY
162bit	6.22e-01	6.22e-01	6.22e-01	6.22e-01
176bit	8.04e-01	8.04e-01	8.04e-01	8.04e-01
192bit	1.28e+00	1.28e+00	1.28e+00	1.28e+00
208bit	1.62e+00	1.62e+00	1.62e+00	1.62e+00
Maragal.6	9.39e+01	9.39e+01	9.39e+01	9.39e+01
Maragal.7	1.33e+02	1.33e+02	1.33e+02	1.33e+02

Table 4: Residual $\|Ax - b\|_F$ of the execution when b is set to ones.

When compared to the results obtained by Cerdán [4], where they also solve the system using a vector b set to ones, it can be seen that the residuals are the same with their Update Preconditioned Method (UPD) and also the non-updated preconditioner method (M) based on the Incomplete Cholesky (IC) factorization (Table 2 of the reference [4]).

Table 5 shows the norm of the solutions x . The norms are all almost equal, with only small differences between our methods and the MKL methods in some cases.

Matrix	Method			
	v33s	v34s	MKL_GELSS	MKL_GELSY
162bit	1.08e+01	1.08e+01	1.04e+01	1.04e+01
176bit	1.50e+01	1.50e+01	1.47e+01	1.47e+01
192bit	2.15e+01	2.15e+01	2.12e+01	2.12e+01
208bit	2.49e+01	2.49e+01	2.47e+01	2.47e+01
Maragal.6	3.64e+05	3.64e+05	3.64e+05	3.64e+05
Maragal.7	1.15e+06	1.15e+06	1.15e+06	1.15e+06

Table 5: Norm of the solution $\|x\|_F$ when b is set to ones.

4.1.4 Scenario 3: Systems with known solution

In this scenario, vector b has been computed as $b = Ax$, where matrix x is randomly generated with values between 0 and 1. Table 6 shows the residuals obtained. As can be seen, in this case, the residuals are much lower than in the previous scenario. The v33s and v34s methods consistently get better residuals than those of the MKL_GELSS method. The v33s and v34s methods get similar residuals to those of the MKL_GELSY method: In some problems, they are slightly higher, and in some problems, they are slightly lower (192bit and 208bit).

Matrix	Method			
	v33s	v34s	MKL_GELSS	MKL_GELSY
162bit	1.66e-12	1.66e-12	6.02e-12	1.18e-12
176bit	3.69e-12	3.69e-12	1.11e-11	3.42e-12
192bit	6.02e-12	6.02e-12	1.72e-10	8.30e-12
208bit	7.51e-12	7.51e-12	1.51e-10	1.19e-11
Maragal.6	1.55e-12	1.55e-12	1.83e-12	6.09e-13
Maragal.7	2.79e-12	2.79e-12	4.00e-12	1.44e-12

Table 6: Residual $\|Ax - b\|_F$ of the execution when x is known.

Table 7 shows the norm of the obtained solution X . As shown, the norms are similar. There is no difference between v33 (T_{12} is annihilated), and v34 (T_{12} is not annihilated).

Matrix	Method			
	v33s	v34s	MKL_GELSS	MKL_GELSY
162bit	3.67e+01	3.67e+01	3.39e+01	3.39e+01
176bit	5.20e+01	5.20e+01	4.85e+01	4.85e+01
192bit	6.82e+01	6.82e+01	6.61e+01	6.61e+01
208bit	8.95e+01	8.95e+01	8.76e+01	8.76e+01
Maragal_6	6.08e+01	6.08e+01	3.93e+01	3.93e+01
Maragal_7	8.36e+01	8.36e+01	5.84e+01	5.84e+01

Table 7: Norm of the solution $\|x\|_F$ when X is known.

To conclude this scenario, when the solution of the system is known, our method based on the randUTV provides consistently good residuals compared to other high-performance linear solvers that work on rank-deficient matrices stored in main memory.

4.1.5 Scenario 4: Systems with vector b perturbed

In this scenario, vector b has been computed as $b = Ax$, where vector x is randomly generated with values between 0 and 1. In contrast with the previous case, the right-hand side b has been perturbed in the following way: 10% of the matrix elements (in random positions) have been set to a 99.9% of the original value.

Table 8 shows the results obtained. As shown, the four methods also obtain the exact same residuals. Compared with other cases, the residuals are higher than in Scenario 3 since vector b has been perturbed. However, the residuals are lower than those obtained in Scenario 2 (b set to ones).

Matrix	Method			
	v33s	v34s	MKL_GELSS	MKL_GELSY
162bit	1.94e-02	1.94e-02	1.94e-02	1.94e-02
176bit	3.32e-02	3.32e-02	3.32e-02	3.32e-02
192bit	4.95e-02	4.95e-02	4.95e-02	4.95e-02
208bit	6.77e-02	6.77e-02	6.77e-02	6.77e-02
Maragal_6	1.73e-02	1.73e-02	1.73e-02	1.73e-02
Maragal_7	2.30e-02	2.30e-02	2.30e-02	2.30e-02

Table 8: Residual $\|Ax - b\|_F$ of the execution when x is known and b has been perturbed (0.1%).

Table 9 shows the norm of the solutions for this scenario. The results show a similar behaviour to all the previous scenarios, where the MKL methods obtain a slightly lower norm, but are not significant.

Matrix	Method			
	v33s	v34s	MKL_GELSS	MKL_GELSY
162bit	3.67e+01	3.67e+01	3.39e+01	3.39e+01
176bit	5.20e+01	5.20e+01	4.85e+01	4.85e+01
192bit	6.82e+01	6.82e+01	6.61e+01	6.61e+01
208bit	8.95e+01	8.95e+01	8.76e+01	8.76e+01
Maragal_6	1.22e+02	1.22e+02	1.12e+02	1.12e+02
Maragal_7	4.18e+02	4.18e+02	4.13e+02	4.13e+02

Table 9: Norm of the solution $\|x\|_F$ when x is known and b has been perturbed (0.1%).

To conclude this precision analysis, we can claim that the numerical stability of the linear least-squares solvers based on the randUTV factorization is up to par with state-of-the-art widely used methods from high-performance high-quality libraries such as Intel MKL. Moreover, the precisions of our methods are also competitive with those of other methods reported in the scientific literature [38, 4]. All these results allow us to claim that our methods as very suitable options for rank-deficient systems, especially if they are of large dimensions.

4.2 Performance analysis

This subsection contains the performance assessment of the new codes described in previous sections, as well as some state-of-the-art codes included and assessed as a reference. To make this study more thorough, the following three architectures have been assessed:

- **volta1 CPU**: A server with 40 cores (Intel Xeon Gold 6138 CPU) at 2.0 GHz and a main memory of 97 GB. The operating system is Debian GNU/Linux 10 (buster). The C compiler is GNU gcc (Debian 8.3.0-6) 8.3.0. The computational library is Intel oneAPI Math Kernel Library Version 2023.0-Product Build 20221128 for Intel 64 architecture applications.
- **volta1 GPU**: Previous machine with a Tesla V100 with 32 GiB of GPU memory. In this case, the Tesla V100 is employed for computational tasks instead of the Intel CPU cores. The computational library is CUDA Release 11.7.
- **mb CPU**: A server with 64 cores (Intel Xeon Platinum 8358 CPU at 2.6 GHz) and a main memory of 263 GB. Note that since it has a larger main memory than the previous one, to exercise the secondary storage system, matrix sizes must be larger. The operating system is Debian GNU/Linux 11 (bullseye). The C compiler is GNU gcc (Debian 10.2.1-6) 10.2.1 20210110. The computational library is Intel oneAPI Math Kernel Library Version 2023.0-Product Build 20221128 for Intel 64 architecture applications. This server has been chosen because it has three different disks:
 - *Spinning disk*: A traditional spinning disk.
 - *SSD disk*: A NVMe (Non-Volatile Memory express) disk.
 - *Optane disk*: A virtual disk implemented on a 1-GiB Intel Optane memory.

In all the experiments below, we have used $q = 0$ (number of steps in the power iteration process), since this number has been usually enough to reveal the rank.

When comparing several methods with different computational costs, the gigaflop rates (gigaflop per second) only report about the efficiency of the codes, and are not useful to assess the overall cost (total time). Since we are going to compare very different methods (QR, SVD, and randUTV) for solving linear systems with different computational costs, all the graphics below employ the scaled time in the vertical axis, unless otherwise stated. The scaled time is computed as the product of the overall time and 10^{12} (to make it more manageable) divided by n^3 , where n is the number of columns, since the computational cost of all methods being assessed in this work is $O(n^3)$.

In all the experiments the block size employed is 10 240, since this is usually the most performant one. Accordingly, all the matrix dimensions assessed in this section are a multiple of this block size. Nevertheless, the methods and all the implementations work on any block size and matrix dimension, even if they are not multiple.

Unless stated otherwise, in all the experiments when solving linear systems below, dimension k (the number of columns of matrix B or the number of linear systems simultaneously being solved) is 1 024.

The block cache size in those variants that use it is 20 GB. Since the dimension of square blocks (those storing data from matrices A , U , and V) is usually $10\,240 \times 10\,240$, the storage of just one of them requires 800 MB when working with double precision. In this case, the block cache could store up to 25 square blocks. In case of blocks of X and B , many more blocks can be stored since their column dimensions are usually smaller.

Analogously, unless stated otherwise, when assessing rank-deficient matrices, the matrix rank for a matrix of dimension $1\,024p$ is $1\,000p$. That is, the rank for a matrix of dimension 81 920 is 80 000, the rank for a matrix of dimension 92 160 is 90 000, and so on. That is, about 2.3 % of the columns are linearly dependent.

The coefficient matrices being assessed in this performance subsection are built as follows. When a matrix of dimension $m \times n$ and numerical rank r must be built, the first step is to build a row block of dimension $r \times n$ with numerical rank r . This is achieved by generating a random block of those dimensions and then making it diagonal-dominant. The second step is to replicate the first block scaled by a random factor as many times as needed to fill the m rows. Note that though this method is very simple, it can be easily scaled up to dimensions so large that the matrices do not fit in main memory.

	v23t	v23c	v23d	v23e	v23x
# Disk Reads	3 799	2 092	2 072	1 567	1 688
# Disk Writes	2 945	1 576	1 558	1 259	1 342

Table 10: Number of disk operations for several OOC variants on the multicore system `volta1` CPU.

4.2.1 Assessment of the block cache systems

Table 10 shows the number of disk operations for several variants when processing a matrix of dimension $92\,160 \times 92\,160$ with rank 90 000 on `volta1` CPU. Recall that variant `v23t` does not employ any block cache, variant `v23c` employs the basic cache with a LRU (Least-Recently-Used) policy, variant `v23d` employs a more sophisticated cache with a LRU policy, and variant `v23e` employs a more sophisticated cache with a LFU (Latest-in-the-Future-to-be-Used) policy. The last variant `v23x` employs the same LFU cache plus overlapping of computation and disk I/O.

As can be seen, the use of a cache greatly reduces the number of disk reads (45 %, from 3 799 to 2 092) and disk writes (46 %, from 2 945 to 1 576). A more advanced cache system further reduces the previous number of disk reads (from 2 092 to 2 072) and disk writes (from 1 576 to 1 558). The new cache system with the LFU eviction policy reduces even more the number of disk reads (from 2 072 to 1 567) and disk writes (from 1 558 to 1 259).

On the other side, although variant `v23x`, which employs overlapping of I/O and computation, also uses the same sophisticated cache system as variant `v23e`, the number of disk operations performed slightly increases. This deserves a close analysis. When overlapping disk I/O and computation, the I/O thread reads blocks in advance. Obviously, from the time a block is read by the I/O thread until that block is processed by the computational thread, that block cannot be chosen to be discarded when trying to load a new block in the cache. This makes that the cache usually contains a set of blocks pending to be “used” that cannot be discarded, thus reducing the effective size of the cache. If the size of the cache is reduced, the effectiveness of the cache is also reduced, thus slightly increasing the number of disk reads and writes.

In overall, the reduction of the number of disk reads and disk writes achieved by the variant with overlapping with respect to the non-cache variant is 56 % (from 3 799 to 1 688) and 54 % (from 2 945 to 1 342).

Identical results were obtained for the variants developed for the GPU architecture, with only slight differences in the variant with overlapping because of the indeterminism introduced by the concurrency of the computational thread and the disk I/O thread.

4.2.2 Decomposed times of variants

	v21t	v22t	v23t	v23s	v33t	v33s
Disk I/O total time	5 158.6	5 685.4	3 984.2	2 005.3	3 996.8	1 957.6
GPU I/O time	—	—	—	—	1 255.9	733.2
Computational time	9 991.3	8 425.1	6 701.8	6 559.0	2 442.5	3 853.6
Added time	15 149.9	14 110.5	10 685.9	8 564.3	7 695.2	6 544.5
Real time	15 389.0	14 366.0	10 862.0	6 639.9	7 799.2	4 906.0

Table 11: Decomposed and real times in seconds for several OOC variants.

Table 11 compares the decomposed and real times of several of our least-squares variants when solving a linear system of dimension $92\,160 \times 92\,160$. Recall that variants `v2xx` are CPU-based, whereas variants `v3xx` are GPU-based. The first data row shows the time spent in disk I/O (transferring data between disk and main memory). The second data row shows the time spent in GPU I/O (transferring data between main memory and the GPU memory), which does not apply for CPU variants. The third data row shows the time spent in computations (either CPU-based or GPU-based). The fourth data row shows the addition of the previous three times. The fifth data row shows the real time.

As can be seen, the real time drops from 15 389.0 seconds (traditional variant `v21t`) to 6 639.9 (fastest CPU variant `v23s`) to 4 906.0 (fastest GPU variant `v33s`). Concretely, by tuning the basic computational tasks, the real time drops 7 % (from 15 389.0 in `v21t` to 14 366.0 in `v22t`). By not building matrix U explicitly, the real time drops 32 % (from 14 366.0 in `v22t` to 10 862.0 in `v23t`). By overlapping I/O and

computation, the real time drops 64 % (from 10 862.0 in `v22t` to 6 639.9 in `v23t`). The GPU variants further reduces the real time by reducing the computational cost. In this case, the reduction is 35 % (from to 6 639.9 to 4 906.0).

4.2.3 Comparison of elementary tasks

	v21t	v22t	v23t	v23s	v33t	v33s
Comp_De	2.346	1.885	1.926	1.759	0.752	1.193
	16	16	16	16	16	16
Comp_TD	13.750	4.946	5.005	5.247	0.987	1.256
	72	72	72	72	72	72
Appl_l_De	2.160	2.393	2.020	1.673	0.366	0.840
	36	36	44	44	44	44
Appl_r_De	2.734	2.331	2.249	2.089	0.413	0.718
	216	216	144	144	144	144
Appl_l_TD	4.613	4.748	4.053	3.459	0.699	1.876
	204	204	240	240	240	240
Appl_r_TD	5.671	4.767	4.959	4.098	0.760	1.715
	972	972	648	648	648	648
Gemm_nn	0.317	0.339	0.300	0.503	0.030	0.030
	117	117	117	117	117	117
Gemm_tn	1.164	1.126	1.375	1.281	0.331	0.557
	365	365	284	284	284	284
Gemm_aabt	1.496	1.476	1.487	1.672	0.370	0.500
	117	117	117	117	117	117
Gemm_abta	1.441	1.434	1.198	1.427	0.276	0.278
	36	36	45	45	45	45
Gemm_aab	1.510	1.474	–	–	–	–
	81	81	–	–	–	–
Svd	92.793	93.890	94.976	109.462	151.100	194.047
	9	9	9	9	9	9
Trsm_lunn	0.163	0.136	0.144	0.193	0.022	0.022
	9	9	9	9	9	9
Comp_RZ	4.582	4.759	4.863	7.589	1.065	0.748
	9	9	9	9	9	9
Appl_r_RZ	1.093	1.184	1.216	4.667	0.718	0.401
	117	117	117	117	117	117
Normal	0.134	0.116	0.117	0.092	0.126	0.098
	44	44	44	44	44	44
Keep_upp	0.059	0.067	0.057	0.067	0.092	0.061
	8	8	8	8	8	8
Zero	0.508	0.532	0.283	0.105	0.292	0.090
	36	36	36	45	36	45
Disk_Read	0.752	0.860	0.731	0.704	0.732	0.826
	4745	4745	3799	1687	3799	1666
Disk_Write	0.426	0.430	0.409	0.608	0.412	0.438
	3738	3738	2945	1344	2945	1328
GPU_Read	–	–	–	–	0.172	0.053
	–	–	–	–	3072	6197
GPU_Write	–	–	–	–	0.154	0.058
	–	–	–	–	4613	6431
# of ops.:	10947	10947	8703	4999	25650	30452

Table 12: Average time in seconds (upper line) and total number of operations (lower line) for every elementary task in several randUTV OOC variants.

Table 12 shows the average time in seconds (upper line) and the number of operations executed (lower line) for every elementary task in several least-squares solver variants. As said before, variant `v21t` is a usual and traditional high-performance implementations based on BLAS-3. In contrast, the rest of CPU variants employ broader (more complex) computational kernels from the Intel MKL library (such as `dlarfb`, `dgeqrf`, `dormqr`, etc.) since they have greatly optimized by this company. As can be seen, the rest of CPU variants achieve higher performances in orthogonal-related tasks such as `Comp_De`, `Comp_TD`, `Appl_l_De`, `Appl_r_De`, `Appl_l_TD`, `Appl_r_TD`, etc. In some cases, the performance gain ranges from a small percentage (such as 16 %) to several times (such as 2.7 times).

Note that the use of overlapping of I/O and computations can slightly increase the computational task in some cases. This slight increase is caused by some interaction between the data transfer and the

computation. Anyway, this increase is clearly compensated by the “hiding” of all the I/O cost.

4.2.4 Comparison of variants

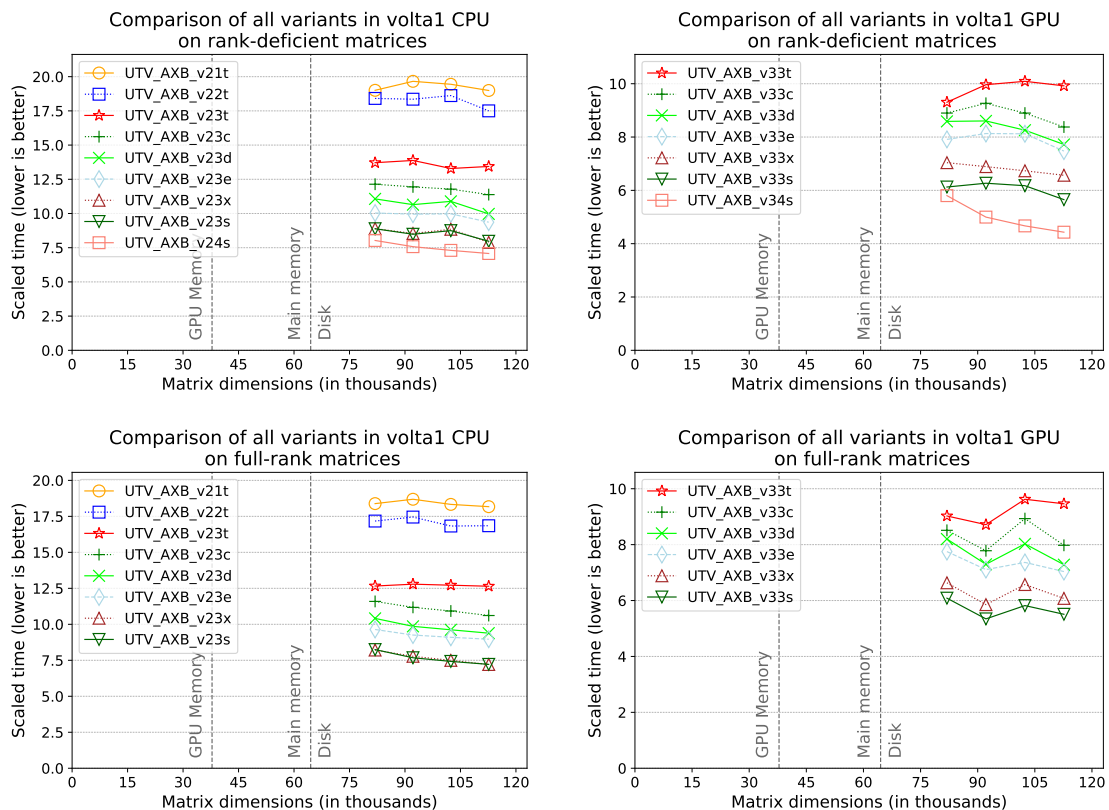


Figure 7: Scaled time versus matrix dimension for all the best least-squares solver variants. The left plots show performances when performing computations on CPU, whereas the right plots show performances when performing computations on GPU. The top plots show results for rank-deficient matrices, whereas the bottom plots show results for full-rank matrices.

Figure 7 shows the scaled time of all of the variants enumerated above with respect to the matrix dimensions. This figure contains four plots as a 2×2 grid: The top plots show the performances on rank-deficient matrices, whereas the bottom plots show the performances on full-rank matrices. The left plots show the performances on a multicore architecture (*volta* CPU), whereas the right plots show the performances on a GPU architecture (*volta* GPU). Obviously, variants that annihilate T_{12} are only shown for rank-deficient matrices, since their performances are the same as the other variants if the matrix is full rank (and therefore T_{12} is empty).

Note that each variant clearly outperforms the previous one. The use of tuned computational CPU kernels in *v22t* variant clearly increases performances with respect to *v21t* variant. In this case, the speed gain derives from the computations exclusively. The *v23t* variant clearly outperform *v22t* variant since the former applies the U orthogonal matrix to matrix B on-the-fly without explicitly building it, thus reducing the overall traffic and computation. The cache variants *v23c* and *v33c* achieve better performances in some cases by reducing the amount of traffic between disk and main memory. On the other hand, variants *v23d* and *v33d* with the new optimized LRU cache improve performances in all cases. Finally, variants with the new LFU cache and overlapping of I/O and computations (*v23x* and *v33x*) are even better. Results of the *v23s* and *v33s* variants show that the use of page-locked memory (*pinned* memory) do not increase performances when working on CPU and slightly increases performances when working on GPU. Variants *v24s* and *v34s* again increase performances, in this case by saving the cost of annihilating block T_{12} .

The plots on GPU performances contain fewer variants since some lessons were taken advantage of from the CPU variants and the running times of the experiments are very large.

To conclude on these four plots, a remarkable performance gain can be seen between the slowest variants and the fastest variants. The performance gain is larger than two when comparing the CPU best variant and the CPU worst variant. On the other hand, the performance gain is about two when comparing the GPU best variant and the GPU worst variant.

4.2.5 Performances with respect to storage devices (disks)

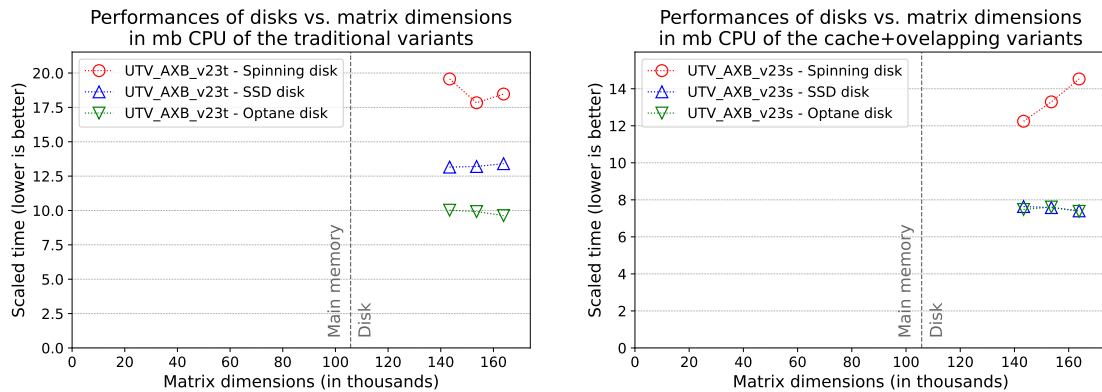


Figure 8: Scaled time versus matrix dimension for the best implementations on several disks for rank-deficient matrices. The left plot shows the results for the traditional variant, whereas the right plot shows the results for the variant with cache and overlapping.

Figure 8 shows the scaled time with respect to matrix dimensions (size of the data) for three different storage devices in **mb CPU**. The left plot shows the results for the traditional variant **v23t** on the three disks, whereas the right plot shows the results for the variant **v23s** (cache and overlapping) on the three disks. When working with the traditional variant (left plot), the SSD disk greatly increases performances with respect to the spinning disk, and again the Optane disk increases performances with respect to the SSD disk. On the other hand, when working with the variant with cache and overlapping (right plot), the SSD disk greatly increases performances with respect to the spinning disk. In this case, the Optane disk does not increase performances and obtains about the same performances than the SSD disk.

4.2.6 Comparison between CPU and GPU implementations

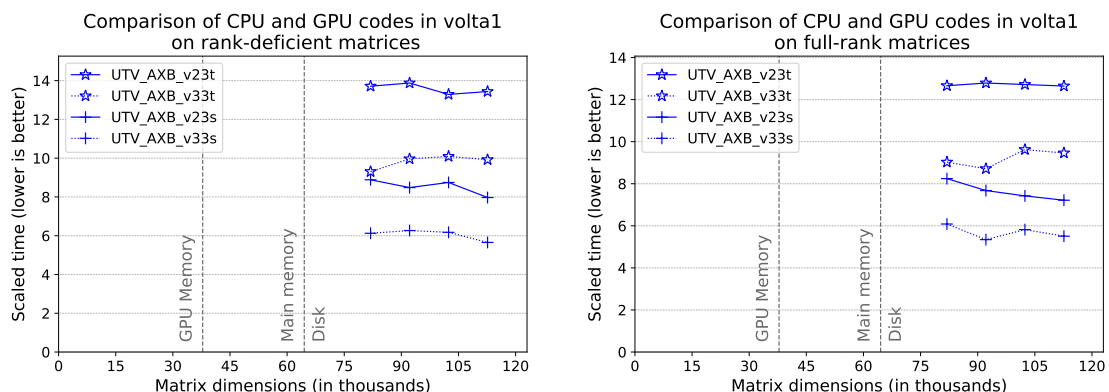


Figure 9: Scaled time versus matrix dimension for the best implementations based on CPU and GPU. The left plot shows performances obtained when processing rank-deficient matrices, whereas the right plot shows performances obtained when processing full-rank matrices.

Figure 9 compares the scaled times of the most-representative CPU-based implementations and the most-representative GPU-based implementations with respect to matrix dimensions. The left plot shows results for rank-deficient matrices, whereas the right plot shows results for full-rank matrices. Comparing

the traditional implementations based on the randUTV factorization, there is a clear performance gap between the GPU implementation (v33t) and the CPU implementation (v23t). Analogously, comparing the implementations with cache and overlapping based on the randUTV factorization, there is a clear performance gap between the GPU implementation (v33s) and the CPU implementation (v23s).

4.2.7 Performances with respect to rank

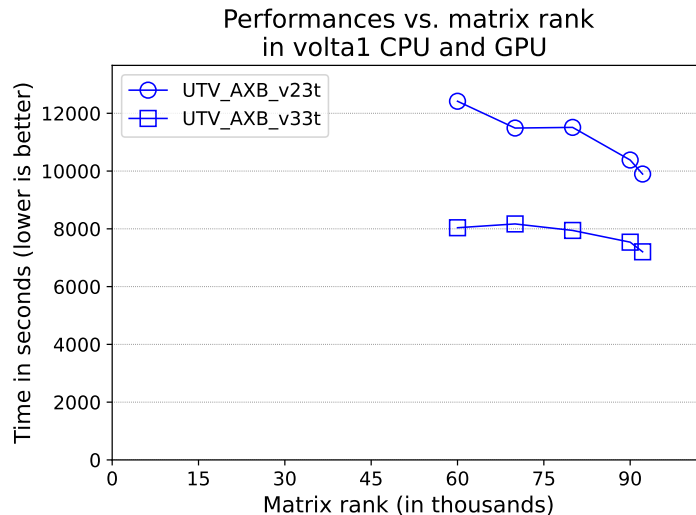


Figure 10: Times in seconds versus matrix rank for several implementations on matrices with different ranks.

Figure 10 shows the total times in seconds of several implementations with respect to matrix rank. Note that the times in this figure are absolute (in seconds) and not scaled. Obviously, the total time depends on the matrix rank since the smaller the rank is, the more elements in T_{12} must be nullified, the higher the computational cost is, and therefore the larger the total time is. In this case, the GPU implementations depend slightly on the matrix rank. On the other side, the CPU implementations do clearly depend on the matrix rank. With respect to the full-rank cost, when the rank is close to half the matrix size, the overall cost only grows about 25 % on CPU and a much smaller percentage on GPU.

4.2.8 Performances with respect to k

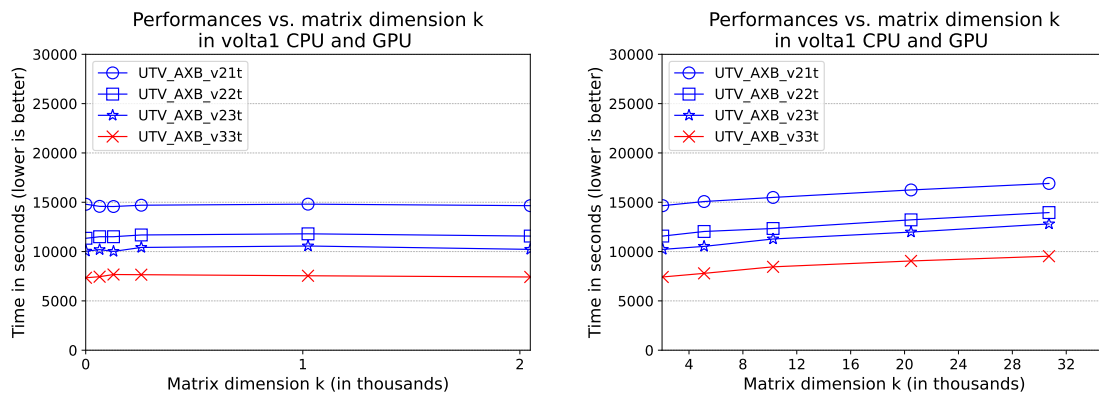


Figure 11: Time in seconds versus matrix dimension k (number of columns in B) for the best implementations for rank-deficient matrices. The left plot shows data up to $k = 2048$, whereas the right plot shows data starting with $k = 2048$.

When solving the problem $\min_X \|AX - B\|$, the number of columns of B also affects the computational cost. Figure 11 shows the performances of the best new implementations with respect to the the number of columns in B (called k). In this case, note that this figure shows the total time in seconds instead of the scaled time since matrix dimensions m and n do not vary. Two plots have been employed to show the performances in more detail. The left plot shows the times in seconds for small values of k (up to 2048), and the right plot shows the times in seconds for larger values of k (starting with 2048). As shown, the total time is about flat for up to 2048 columns in B , and it only increases slightly starting with 2048 columns. Note that the case with 30 720 columns is only slightly slower than the case with one column. Examining the data in more detail, the worst variant, `v21t`, requires 14 796 and 16 907 seconds for $k = 1$ and $k = 30\,720$, respectively, which is a 14.3 % increment when solving 30 720 times as many systems.

4.2.9 Comparison of In-Core codes and OOC codes

Several high-performance In-Core implementations have been assessed and included here as a reference to our new Out-Of-Core implementations. When high-performance In-Core implementations from commercial or open-source libraries were available, they were assessed. When not available, we implemented them using high-performance commercial or open-source libraries. We have assessed the following In-Core codes:

- `MKL.GELS`: High-performance linear least squares solver `dGELS` from the Intel MKL library. As it is based on the QR factorization, it does not work on rank-deficient matrices. Obviously, this code has been only assessed with full-rank matrices.
- `MKL.GELSY`: High-performance linear least squares solver `dGELSY` from the Intel MKL library. It can process rank-deficient matrices since it is based on the column-pivoting QR factorization.
- `MKL.GELSS`: High-performance linear least squares solver `dGELSS` from the Intel MKL library. It can process rank-deficient matrices since it is based on the SVD factorization.
- `UTV_AXB_v11`: High-performance implementation for solving systems with data stored in main memory (In-Core computations) based on the `randUTV` factorization. It employs BLAS-3 from the Intel MKL library. It can work on rank-deficient matrices.
- `CUSOLVER_QR_LS`: High-performance implementation for GPU analogous to `MKL.GELS`. Since there is not a linear least-squares implementation in the NVIDIA `cuSOLVER` library based on the QR factorization, we have implemented it using the `dgeqrf`, `dormqr`, and `dtrsm` routines from the high-performance NVIDIA `cuSOLVER` library. As it is based on the QR factorization, it does not work on rank-deficient matrices. In this case, this code has been assessed with full-rank matrices of the corresponding dimensions.
- `CUSOLVER_SVD_LS`: High-performance implementation for GPU analogous to `MKL.GELSS`. This implementation is based on the high-performance NVIDIA `cuSOLVER` library. Since there is not a linear least-squares implementation in `cuSOLVER` based on the SVD factorization, we have also implemented it using the `xgesvd`, `dgemm`, and `dtrsm` routines from the high-performance NVIDIA `cuSOLVER` library. As it is based on the SVD factorization, it can work on rank-deficient matrices.

Figure 12 compares our new OOC implementations that can process data so large that must be stored in the hard drive versus state-of-the-art high-performance implementations that only work on data stored in main memory. The left plot shows the performances on a CPU architecture, whereas the right plot shows the performances on a GPU architecture. Continuous lines are used for codes that can process rank-deficient matrices. Non-continuous lines are used for codes that can only process full-rank matrices, and are included just as a reference (and are usually faster). Codes with continuous lines have been assessed on rank-deficient matrices with the corresponding ranks for the corresponding dimensions ($10\,000k$ rank for $10\,240k$ dimensions), as described before. Codes with non-continuous lines have been assessed on full-rank matrices with the corresponding dimensions since they do not work on rank-deficient matrices.

In each plot, the lines in the left are the In-Core implementations, that is, implementations that can only work on data stored in the more expensive (and limited) main memory. Accordingly, in each plot, the lines in the right are our new OOC implementations, which can work on matrices of any size, even though they do not fit in main memory and must be stored in the hard drive.

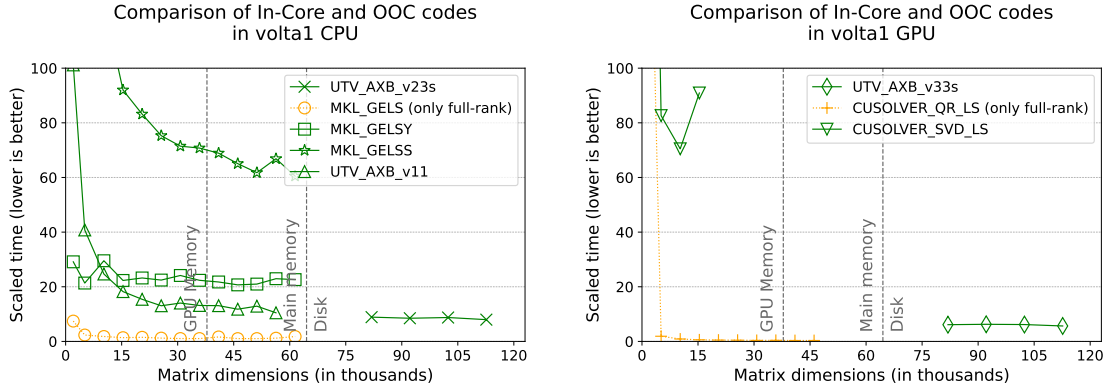


Figure 12: Scaled time versus matrix dimensions for the best implementations for rank-deficient matrices. The left plot shows the performances of CPU codes, whereas the right plot shows the performances of GPU codes. Both plots include both In-Core codes (left side of both plots) and Out-Of-Core codes (right side of both plots).

As shown, our new OOC implementation on a CPU architecture are so fast that they can outperform high-performance implementations from the Intel MKL library. Our OOC implementation obtains a speed very similar to the In-Core implementation that has all the data in main memory. As can be seen on the right plot (GPU-based architectures), our code is faster than an In-Core implementation based on the cuSOLVER library. The right plot shows results for the implementation based on the SVD factorization from cuSOLVER up to $n = 15k$ since its convergence fails for $n \geq 20k$. Note that in both plots, implementations based on the QR factorization are obviously much faster, but you must recall that they only work on full-rank matrices.

5 Conclusions

Solving very large linear systems of equations is a crucial task in many problems from science and technology. In many cases, the coefficient matrix of the system is rank-deficient, and usual methods for full-rank matrices cannot be applied. When the coefficient matrix of the system is rank-deficient, the linear systems may be underdetermined, inconsistent, or both. In such cases, one generally seeks to compute the least squares solution that minimizes the residual of the problem, and is further defined as the solution with smallest norm in cases where the coefficient matrix has a nontrivial nullspace.

This work introduces several new techniques for solving least squares problems with coefficient matrices that are so large that they do not fit in main memory and must be stored in the disk drive.

All techniques rely on complete orthogonal factorizations that guarantee that both conditions of a least squares solution are met, regardless of the rank properties of the matrix. That is, our new methods can solve linear systems with both full-rank and rank-deficient coefficient matrices, for both consistent and inconsistent problems. Specifically, they rely on the recently proposed “randUTV” algorithm that is particularly effective in strongly communication-constrained environments. Our work accelerates the speed of previous Out-Of-Core implementations of the randUTV factorization by introducing several performance improvements. Moreover, new high-performance implementations for GPU were developed.

A detailed precision study of our new implementations has been performed, which includes both our own matrices and several large matrices from public repositories. The precision of the new codes is competitive with those of methods working in main memory.

A thorough performance study of the codes for solving the linear least squares problem has been performed. The performances of the new codes, that operate on data stored on disk, are competitive with current high-performance methods that work only on data stored in main memory (thus limited in size).

The performances of our new codes are slower than those of specific methods for full-rank matrices, but only slightly so. Our new methods can be employed both in CPU architectures and GPU architectures, delivering good performance and precision in both cases.

Acknowledgements

G. Quintana-Ortí, M. Chillarón, and V. Vidal were supported the TED2021-131091B-I00 research project, funded by MCIN/AEI/10.13039/501100011033 and by the “European Union NextGenerationEU/PRTR”. M. Chillarón and V. Vidal were also supported by “Universitat Politècnica de València”. P.G. Martinsson acknowledges support from the Office of Naval Research (N00014-18-1-2354), the National Science Foundation (DMS-2313434 and DMS-1952735), the Department of Energy ASCR (DE-SC0022251), and the Texas Advanced Computing Center. The authors would like to thank Francisco D. Igual (Universidad Complutense de Madrid) for granting access to the `volta1` and the `mb` servers.

References

- [1] Emmanuel Agullo, Alfredo Buttari, Abdou Guermouche, and Florent Lopez, *Task-based multifrontal QR solver for GPU-accelerated multicore architectures*, 2015 IEEE 22nd international conference on high performance computing (HiPC), IEEE, 2015, pp. 54–63.
- [2] Amir Beck and Marc Teboulle, *A fast iterative shrinkage-thresholding algorithm for linear inverse problems*, SIAM journal on imaging sciences **2** (2009), no. 1, 183–202.
- [3] Peter Businger and Gene H. Golub, *Linear least squares solutions by householder transformations*, Numerische Mathematik **7** (1965), no. 3, 269–276.
- [4] Juana Cerdán, Daniel Guerrero, José Marín, and José Mas, *Preconditioners for rank deficient least squares problems*, Journal of Computational and Applied Mathematics **372** (2020), 112621.
- [5] Mónica Chillarón, Gregorio Quintana-Ortí, Vicente Vidal, and Gumersindo Verdú, *Computed tomography medical image reconstruction on affordable equipment by using Out-Of-Core techniques*, Computer Methods and Programs in Biomedicine **193** (2020), 105488.
- [6] Timothy A Davis and Yifan Hu, *The university of florida sparse matrix collection*, ACM Transactions on Mathematical Software (TOMS) **38** (2011), no. 1, 1–25.
- [7] Eduardo D’Azevedo and Jack Dongarra, *The design and implementation of the parallel out-of-core scalapack lu, qr, and cholesky factorization routines*, Concurrency: Practice and Experience **12** (2000), no. 15, 1481–1493.
- [8] Vadim Demchik, Miroslav Bacák, and Stefan Bordag, *Out-of-core singular value decomposition*, CoRR **abs/1907.06470** (2019).
- [9] Zlatko Drmač and Zvonimir Bujanović, *On the failure of rank-revealing qr factorization software – a case study*, ACM Trans. Math. Softw. **35** (2008), no. 2.
- [10] Gennady Fedorov and Mariia Zhukova, *Multifrontal Sparse QR Factorization Method for Solving a Sparse System of Linear Equations*, 2018.
- [11] David Chin-Lung Fong and Michael Saunders, *LSMR: An iterative algorithm for sparse least-squares problems*, SIAM Journal on Scientific Computing **33** (2011), no. 5, 2950–2971.
- [12] Massimo Fornasier, Steffen Peter, Holger Rauhut, and Stephan Worm, *Conjugate gradient acceleration of iteratively re-weighted least squares methods*, Computational optimization and applications **65** (2016), 205–259.
- [13] Leslie V Foster and Timothy A Davis, *Algorithm 933: Reliable calculation of numerical rank, null space bases, pseudoinverse solutions, and basic solutions using SuiteSparseQR*, ACM Transactions on Mathematical Software (TOMS) **40** (2013), no. 1, 1–23.
- [14] Gene Golub and William Kahan, *Calculating the singular values and pseudo-inverse of a matrix*, Journal of the Society for Industrial and Applied Mathematics, Series B: Numerical Analysis **2** (1965), no. 2, 205–224.
- [15] Gene H. Golub and Charles F. Van Loan, *Matrix computations*, third ed., Johns Hopkins Studies in the Mathematical Sciences, Johns Hopkins University Press, Baltimore, MD, 1996.

- [16] B.C. Gunter, W.C. Reiley, and R.A. van de Geijn, *Parallel out-of-core cholesky and qr factorizations with poclpack*, Proceedings 15th International Parallel and Distributed Processing Symposium. IPDPS 2001, 2001, pp. 1885–1894.
- [17] Brian C Gunter and Robert A Van De Geijn, *Parallel out-of-core computation and updating of the QR factorization*, ACM Transactions on Mathematical Software (TOMS) **31** (2005), no. 1, 60–78.
- [18] Nathan Halko, Per-Gunnar Martinsson, Yoel Shkolnisky, and Mark Tygert, *An algorithm for the principal component analysis of large data sets*, SIAM Journal on Scientific computing **33** (2011), no. 5, 2580–2594.
- [19] Nathan Halko, Per-Gunnar Martinsson, and Joel A. Tropp, *Finding structure with randomness: Probabilistic algorithms for constructing approximate matrix decompositions*, SIAM Review **53** (2011), no. 2, 217–288.
- [20] Eric Hallman and Ming Gu, *LSMB: Minimizing the backward error for least-squares problems*, SIAM Journal on Matrix Analysis and Applications **39** (2018), no. 3, 1295–1317.
- [21] N. Heavner, F. D. Igual, G. Quintana-Ortí, and P. G. Martinsson, *Algorithm 1022: Efficient algorithms for computing a rank-revealing utv factorization on parallel computing architectures*, ACM Trans. Math. Softw. **48** (2022), no. 2, 1–42.
- [22] N. Heavner, P. G. Martinsson, and G. Quintana-Ortí, *Computing rank-revealing factorizations of matrices stored out-of-core*, Concurrency and Computation: Practice and Experience (2023), e7726.
- [23] Nathan Heavner, Chao Chen, Abinand Gopal, and Per-Gunnar Martinsson, *Efficient algorithms for computing rank-revealing factorizations on a gpu*, Numerical Linear Algebra with Applications **30** (2023), no. 6, e2515.
- [24] Patricia D Hough and Stephen A Vavasis, *Complete orthogonal decomposition for weighted least squares*, SIAM Journal on Matrix Analysis and Applications **18** (1997), no. 2, 369–392.
- [25] K. Kabir, A. Haidar, S. Tomov, A. Bouteiller, and J. Dongarra, *A framework for out of memory svd algorithms*, High Performance Computing. ISC 2017 (J. Kunkel, R. Yokota, P. Balaji, and D. Keyes, eds.), Lecture Notes in Computer Science, vol. 10266, Springer Berlin Heidelberg, 2017.
- [26] Na Li and Yousef Saad, *MIQR: A multilevel incomplete QR preconditioner for large sparse least-squares problems*, SIAM journal on matrix analysis and applications **28** (2006), no. 2, 524–550.
- [27] Edo Liberty, Franco Woolfe, Per-Gunnar Martinsson, Vladimir Rokhlin, and Mark Tygert, *Randomized algorithms for the low-rank approximation of matrices*, Proc. Natl. Acad. Sci. USA **104** (2007), no. 51, 20167–20172.
- [28] P. G. Martinsson, G. Quintana-Ortí, and N. Heavner, *Randutv: A blocked randomized algorithm for computing a rank-revealing utv factorization*, ACM Trans. Math. Softw. **45** (2019), no. 1, 4:1–4:26.
- [29] Per-Gunnar Martinsson, Vladimir Rokhlin, and Mark Tygert, *A randomized algorithm for the decomposition of matrices*, Appl. Comput. Harmon. Anal. **30** (2011), no. 1, 47–68. MR 2737933 (2011i:65066)
- [30] Christopher C Paige and Michael A Saunders, *LSQR: An algorithm for sparse linear equations and sparse least squares*, ACM Transactions on Mathematical Software (TOMS) **8** (1982), no. 1, 43–71.
- [31] Gregorio Quintana-Ortí, Mónica Chillarón, Vicente Vidal, and Gumersindo Verdú, *High-performance reconstruction of CT medical images by using out-of-core methods in GPU*, Computer Methods and Programs in Biomedicine **218** (2022), 106725.
- [32] Gregorio Quintana-Ortí, Francisco D Igual, Mercedes Marqués, Enrique S Quintana-Ortí, and Robert A Van de Geijn, *A runtime system for programming out-of-core matrix algorithms-by-tiles on multithreaded architectures*, ACM Transactions on Mathematical Software (TOMS) **38** (2012), no. 4, 25.
- [33] ———, *A runtime system for programming out-of-core matrix algorithms-by-tiles on multithreaded architectures*, ACM Transactions on Mathematical Software (TOMS) **38** (2012), no. 4, 25.

- [34] Gregorio Quintana-Ortí, Enrique S. Quintana-Ortí, and Antoine Petitet, *Efficient solution of the rank-deficient linear least squares problem*, SIAM Journal on Scientific Computing **20** (1998), no. 3, 1155–1163.
- [35] Gregorio Quintana-Ortí, Xiaobai Sun, and Christian H Bischof, *A blas-3 version of the qr factorization with column pivoting*, SIAM Journal on Scientific Computing **19** (1998), no. 5, 1486–1494.
- [36] Wesley C Reiley and Robert A Van De Geijn, *Pooclapack: Parallel out-of-core linear algebra package*, University of Texas at Austin, Austin, TX (1999).
- [37] Yousef Saad, *Iterative methods for sparse linear systems*, SIAM, 2003.
- [38] Jennifer Scott, *On using Cholesky-based factorizations and regularization for solving rank-deficient sparse linear least-squares problems*, SIAM Journal on Scientific Computing **39** (2017), no. 4, C319–C339.
- [39] Jennifer Scott and Miroslav Tůma, *Solving mixed sparse-dense linear least-squares problems by preconditioned iterative methods*, SIAM Journal on Scientific Computing **39** (2017), no. 6, A2422–A2437.
- [40] ———, *A computational study of using black-box qr solvers for large-scale sparse-dense linear least squares problems*, ACM Transactions on Mathematical Software (TOMS) **48** (2022), no. 1, 1–24.
- [41] Wissam Sid-Lakhdar, Sebastien Cayrols, Daniel Bielich, Ahmad Abdelfattah, Piotr Luszczek, Mark Gates, Stanimire Tomov, Hans Johansen, David Williams-Young, Timothy Davis, Jack Dongarra, and Hartwig Anzt, *Paqr: Pivoting avoiding qr factorization*, 2023 IEEE International Parallel and Distributed Processing Symposium (IPDPS), 2023, pp. 322–332.
- [42] Sivan Toledo and Fred G Gustavson, *The design and implementation of solar, a portable library for scalable out-of-core linear algebra computations*, IOPADS, vol. 96, Citeseer, 1996, pp. 28–40.
- [43] Sencer Nuri Yeralan, Timothy A Davis, Wissam M Sid-Lakhdar, and Sanjay Ranka, *Algorithm 980: Sparse QR factorization on the GPU*, ACM Transactions on Mathematical Software (TOMS) **44** (2017), no. 2, 1–29.